Studies on structural, electrical, and optical properties of Cu doped As–Se–Te chalcogenide glasses

Juejun Hu, Xiaochen Sun, Anuradha M. Agarwal,[a] Jean-Francois Viens, and Lionel C. Kimerling
Materials Processing Center, MIT, Cambridge, Massachusetts 02139

Laeticia Petit, Nathan Carlie, and Kathleen C. Richardson
School of Materials Science and Engineering, Clemson University, Clemson, South Carolina 29634

Troy Anderson, Jiyeon Choi, and Martin Richardson
College of Optics and Photonics CREOL/FPCE, University of Central Florida, Orlando, 4000 Central Florida Boulevard, Florida 32816

(Received 27 September 2006; accepted 19 January 2007; published online 23 March 2007)

Cu doped chalcogenide (ChG) glassy films in the As–Se–Te glass system have been prepared using thermal evaporation techniques. Single-source evaporation from bulk $(1-x)$ $As_{0.40}Se_{0.35}Te_{0.25}+x$ Cu glasses with $x=0.05$, 0.075, 0.10, 0.125, and 0.15, as well as dual-source coevaporation from As-chalcogenide and Cu-chalcogenide binary glasses as source materials, has been explored. We have shown that it is not possible to deposit high concentration Cu doped ChG glassy films, from the Cu doped bulk samples using single-source evaporation. However, using the dual-source coevaporation technique, we have demonstrated that the films can be doped with high concentrations of Cu. Micro-Raman spectroscopy has been utilized to verify that Cu is introduced into the glass network without disrupting the basic As-chalcogen units. Optical measurements have shown that introduction of Cu decreases the band gap of As–Se–Te glasses. The electrical properties of the investigated films have been measured at different temperatures and it has been shown that Cu incorporation in the As–Se–Te glass system vastly improves electrical conductivity. Moreover, we have shown that the temperature dependence of electrical conductivity can be fitted assuming variable range hopping between states near the Fermi level. © *2007 American Institute of Physics*. [DOI: 10.1063/1.2712162]

I. INTRODUCTION

A rising interest in the possible use of electrochemical sensors for miniaturized devices has lead to their extensive study in recent years. Chalcogenide (ChG) glasses with their flexible structure, enormous variation in properties, and almost unlimited ability for doping and alloying are promising materials for chemical sensors in the analysis of industrial aqueous solutions and to monitor pollutant gases in the environment.[1] Moreover, ChG glasses are conducive for use in fiber optics and integrated optics since they have many unique optical properties and exhibit a good transparency in the infrared region.[2,3] Because of their IR transparency, photosensitivity, high optical nonlinearity, and rare-earth doping potential, these glasses have been utilized to fabricate photonic devices such as fibers,[4] planar waveguides,[5,6] gratings,[7] all-optical switches,[8] and fiber amplifiers.[9]

As_2S_3 and As_2Se_3 have traditionally been used for mid-IR fibers with transmission windows up to 12 μm. In order to further the transmission window into the far-IR range (>15 μm), the S or Se atoms, which cause far-IR absorption due to As–S or As–Se bond vibration, can be replaced by heavier counterparts such as Te or transition metals. Chalcogenide glasses containing metal atoms have optical and electronic properties which are different from those of the ordinary chalcogenide glasses. In recent years, transition metal (e.g., Cu, Ag, Sn, and Cr) doped chalcogenide glasses have been used as optical memory[10] and laser[11] materials. Some previous investigations[12] have shown that the introduction of Cu into the As_2Se_3 glass causes a substantial increase in the efficiency (contrast, photosensitivity, reversibility, and diffractive efficiency) of optical recording on thin films of $Cu_x(As_2Se_3)_{100-x}$ with $x<20$ at. %. In addition, Cu doped chalcogenide glasses and films exhibit photoconductivity and band gap shrinkage with increasing Cu doping, suggesting their potential application in low-cost mid-IR detection, which necessitates the investigation of their electrical properties, and their ability to appropriately modify the band structure.[13]

For many of these applications, thin films are necessary. The wide practical application of thin amorphous chalcogenide films, especially of the vitreous As-containing condensates, is closely connected with their transparency in the visible and near IR spectral regions and with the possibility to create optical media with defined values of the refractive index, dispersion, and extinction coefficients. The relatively low energy of the chemical bonds in the As-based chalcogenide glasses offers the opportunity for photostructural transformations and a number of other light-induced effects, all of which are typically accompanied by considerable changes in the chalcogenide's optical constants.[14] Many methods for thin film preparation have been demonstrated. Some include

[a]Electronic mail: anu@mit.edu

spin coating, evaporation of one or more materials at low pressures and high temperature in vacuum, ionic and magnetron sputtering, pulsed laser deposition, and chemical vapor deposition. The preparation of chalcogenide thin films of complex compositions can be a difficult task and classical deposition methods cannot often be used to form films with a strict stoichiometric match to the target.

In this paper we evaluate two film deposition techniques for the preparation of films from As–Se–Te glasses containing high concentrations of Cu: thermal evaporation (single-source evaporation) and coevaporation. The first technique for the film deposition is the thermal evaporation technique from bulk Cu doped chalcogenide glasses, where the bulk material is used as the target. A systematic study of the structural modification of the chalcogenide bulk glasses in the ternary system As–Se–Te with the progressive introduction of Cu across a broad glass-forming range is presented. We establish a correlation between the glass structure and the optical properties of the glasses as determined from chemical and physical property measurements. Raman scattering has been used to examine the glass structure modification as a function of Cu concentration in the arsenic based glass system, using both single-source and dual-source coevaporated films. The composition of the films has been verified using wavelength dispersive spectroscopy (WDS) and the structure of the different films has been measured using micro-Raman spectroscopy. The electrical properties of the Cu doped bulk and films have been investigated. A study of the electrical conductivity as a function of temperature has been used as a powerful tool to probe the electronic transport mechanism in the glasses.

II. EXPERIMENT

A. Sample preparation

1. Bulk elaboration

Glasses with nominal compositions of $(1-x)$ $As_{0.40}Se_{0.35}Te_{0.25}+x$ Cu with $x=0.05$, 0.075, 0.10, 0.125, and 0.15 were prepared in a 6 g batch by melting in sealed containers and stored in a dry nitrogen environment within a glovebox prior to use. The glasses were prepared from high purity elements (As: Aldrich 99.999%; Se: Cerac 99.999%; Te: Cerac 99.999%; and Cu: Alfa 99.999%). Starting materials were weighed and batched inside a nitrogen-purged glovebox and sealed into quartz ampoules using a gas-oxygen torch under vacuum. Prior to sealing and melting, the ampoule and batch were preheated at 100 °C for 4 h to remove surface moisture from the quartz ampoule and the batch raw materials. The ampoule was then sealed and heated for 24 h to between 800 and 950 °C, depending on the glass composition. A rocking furnace was used to rock the ampoule during the melting to increase the homogeneity of the melt. Once homogenized, the melt-containing ampoule was air quenched to room temperature. To avoid fracture of the tube and glass ingot, the ampoules were subsequently returned to the furnace for annealing for 15 h at 40 °C below the glass transition temperature T_g. The same procedure was used for Se-substituted compositions.

The glass samples were then cut, optically polished, and inspected visually. The compositions were checked by WDS using a JEOL JXA-733 superprobe and were found to be identical to the initial concentrations introduced in the batch.

2. Film deposition

Chalcogenide glass thin films were deposited on both oxide coated Si wafers (4 in. Si wafers with 1 μm thermal oxide, Silicon Quest International) as well as precleaned glass microscope slides (VWR International) by thermal evaporation. Films on the two different substrates were found to have very similar material properties due to the amorphous nature of both substrates at the substrate-film interface. Two different evaporation techniques, single-source evaporation from Cu doped bulk glasses and dual-source coevaporation of As_2Se_3 or As_2Te_3 (Alfa Aesar Inc., 99.99%) and CuSe (Alfa Aesar Inc., 99.99%), were tested. The evaporations were carried out with a base pressure of $<10^{-6}$ Torr. During evaporation, the current and voltage on the molybdenum boats are monitored to bring the chalcogenides just above melting point in order to establish a vapor pressure in the chamber and keep a constant evaporation rate. In dual-source coevaporation, ratios of coevaporated components are achieved by controlling the current passing through the individual boats. In the coevaporation scheme, depositions were carried out only when the evaporation reached a steady state, namely, a constant deposition rate is maintained at a fixed current value in order to equilibrate the evaporation sources.

B. Property measurement

The glass transition temperatures (T_g) were determined by differential scanning calorimetry (DSC) at a heating rate of 10 °C/min from 50 to 500 °C using a commercial DSC apparatus. The measurements were carried out in a hermetically sealed aluminum pan.

The density of bulk glass materials was measured by Archimedes' principle using diethylphtalate. The accuracy was better than ± 0.02 g/cm^3.

C. Absorption spectra

Transmittance spectra recorded in the range of 1100–2500 nm were taken on a Cary 5E UV-Vis-NIR dual-beam spectrophotometer. Using the film transmission spectra, it is possible to determine the refractive index dispersion and the thickness of the films. However, for this paper, only a comparison of the transmission spectra is presented.

D. Structural characterization

The Raman spectra were recorded with a Kaiser Hololab 5000R Raman spectrometer with Raman microprobe attachment (typical resolution of 2–3 cm^{-1}) in backscattering geometry at room temperature. The system consists of a holographic notch filter for Rayleigh rejection, a microscope equipped with 10×, 50×, and 100× objectives (the latter allowing a spatial resolution of less than 2 μm) and a charge-coupeld device (CCD) detector. A 785 nm line of a Ti:sapphire laser was used for excitation with incident power

of around 2 mW. The use of a 785 nm source with a low power was deemed essential to our study to avoid photostructural changes that laser beam may induce in the samples.

E. Femtosecond laser irradiation setup

The laser oscillator used for the writing process in this study is an extended-cavity Ti:sapphire laser with a repetition rate reduced to 35.8 MHz and an ~25 nm spectral bandwidth centered at 810 nm that produces 8 nJ pulses with 62 fs duration and 6% pulse-to-pulse stability. The Gaussian laser output beam (M^2 of ~2.6) was focused by a 10×, 0.25 numerical aperture (NA) microscope objective at the surface of the bulk sample that was translated perpendicular to the laser beam by a computer-controlled three-axis translation stage. The laser intensity was adjusted with a variable metallic neutral-density filter placed before the microscope objective. The resulting photomodified surface profile was then analyzed with a white-light interference microscope (Zygo Instrument NewView5000) to assess photoinduced surface modification.

F. Electrical measurements

Before electrical measurements, Ohmic contacts were obtained by evaporation of tin electrodes onto the sample surface through a metal shadow mask, using an Edwards 306A resistive vacuum evaporator. Current-voltage (*I-V*) curves at different temperatures were measured. Voltage was applied through a pair of metal probes and the current flowing through the two metal pads was recorded. The (*I-V*) measurements were conducted using a Bio-Rad DL8000 digital DLTS system from low temperature up to about 200 K. Conductivity at different temperatures was extracted by least squares linear fit of the (*I-V*) data. The error of the measurement is estimated to be smaller than 1 pS.

Important information regarding the charge transport mechanism, which is still an issue of debate, can be probed through measuring material conductivity at different temperatures. Different models have been proposed to explain the temperature dependence of electrical conductivity in amorphous materials, among which the Mott-Davis model has been the most successful for chalcogenide glasses to date.[15] According to this model, three mechanisms may dominate electrical conduction in amorphous materials at different temperatures: (i) extended state conduction, (ii) thermal excitation of localized states near the mobility edge, and (iii) variable range hopping between states near the Fermi level. The first two mechanisms are characterized by the Arrhenius equation while variable range hopping obeys the well-known $T^{1/4}$ law,

$$\sigma = \sigma_0 \exp\left(\frac{T_0}{T}\right)^{-1/4}, \tag{1}$$

where σ and T represent electrical conductivity and temperature in kelvins, respectively, and σ_0 and T_0 are two constants that relate material band structures to electrical properties.

TABLE I. Variation in glass transition temperature, density, and conductivity of the investigated bulk samples used in the single-source film evaporation, as a function of atomic fraction of Cu in the glass host system $(1-x)$ $As_{0.40}Se_{0.35}Te_{0.25}+x$ Cu.

Atomic fraction Cu (x)	Glass transition temperature T_g (°C) ±5 °C	Density (g/cm^3) ±0.02	Conductivity [1/(Ω m)] at 298 K
0		4.99	
0.05		5.18	
0.075	157	5.25	0.000 56
0.1	162	5.30	0.001 52
0.125	168	5.40	0.005 18
0.15	174	5.35	0.019 49

III. RESULTS AND DISCUSSION

The aim of this study was the preparation and characterization of As–Se–Te–Cu glass films. Thermal evaporation from one or more bulk sources is a process kinetically controlled by the partial pressure of vapors. Two methods, single-source evaporation from bulk $(1-x)$ $As_{0.40}Se_{0.35}Te_{0.25}+x$ Cu glasses with $x=0.05$, 0.075, 0.10, 0.125, and 0.15 and dual-source coevaporation from As-chalcogenide and Cu-chalcogenide glasses, are both used for glass film deposition. Raman spectroscopy has been employed to evaluate structural modifications in the films, and this result is complemented by characterization of structural sensitive properties such as T_g and electrical conductivity.

A. Single-source thermal evaporation of Cu doped films in the system $As_{0.40}Se_{0.35}Te_{0.25}$

Cu doped films were obtained by single-source thermal deposition technique using Cu doped glasses in the composition of $(1-x)$ $As_{0.40}Se_{0.35}Te_{0.25}+x$ Cu with $x=0.075$, 0.10, 0.125, and 0.15 used as a source.

1. Source characterization

In Table I we report the glass transition temperatures and the density of the Cu doped $As_{0.40}Se_{0.35}Te_{0.25}$ glasses as a function of Cu content. The glass transition temperatures of the glasses with the composition of $(1-x)$ $As_{0.40}Se_{0.35}Te_{0.25}$ $+x$ Cu with $x=0.05$, 0.075, 0.10, 0.125, and 0.15 increase monotonically with increasing Cu incorporation and the corresponding density increases from 4.99 to 5.35 g/cm^3. The absence of sharp diffraction peaks in the XRD spectra has confirmed the amorphous nature of the glasses and lack of detectable crystallinity for the Cu doping levels used.

The absorption spectra of the glasses are shown in the Fig. 1. When Cu is gradually added in the glass network, the optical band gap exhibited a shift to the near infrared. The exponential absorption tail of the bulk glasses can be well fitted by an Urbach band tail model, which confirms the existence of midgap states in these amorphous materials.

The micro-Raman spectra of the glass with $x=0.15$, taken as an example, is presented in Fig. 2. The spectra exhibit a broad band from 100 to 300 cm^{-1}. No variation of the Raman signal was observed when the Cu content increases.

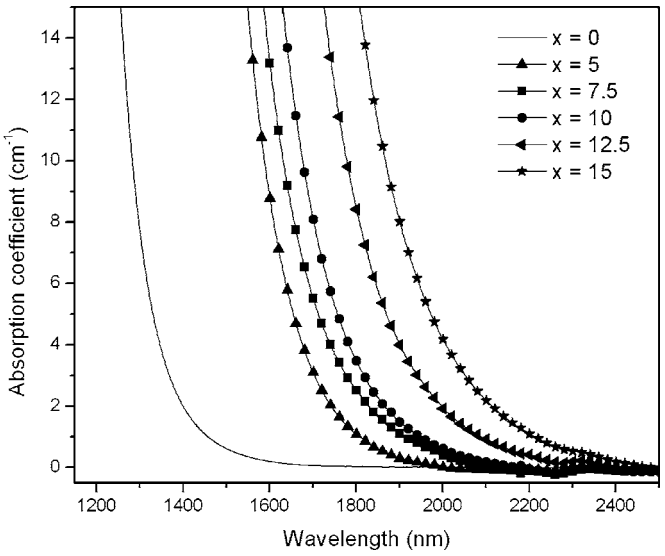

FIG. 1. Absorption spectra of bulk $(1-x)$ $As_{0.40}Se_{0.35}Te_{0.25}+x$ Cu glasses. When Cu is gradually added in the glass network, the optical band gap exhibits a shift to the near infrared.

This may suggest that Cu is introduced into the glass without disrupting the basic network units, i.e., As-chalcogen pyramids. The major Raman peak is centered near 195 cm^{-1} for all samples. The main broad band cannot be simply attributed to $AsSe_3$ pyramids [typical vibration band located at 200–280 cm^{-1} (Ref. 16)] or $AsTe_3$ units [typical vibration band located at 150–190 cm^{-1} (Ref. 17)]. In accordance with Nguyen *et al.*, this band may be attributed to modified structural units which are represented by $AsSe_{(3-x)}Te_x$ structural units.[18] The shoulders at smaller wave number may be attributed to greater Te concentrated $AsSe_{(3-x)}Te_x$ units, as Te is heavier than Se. The shoulder at 170 cm^{-1} is consistent with the features that appear in pure As_2Te_3 glasses and is probably due to $AsTe_3$ units existing in the glasses, whereas the shoulder at ~240 cm^{-1} may be related to $AsSe_3$ pyramidal units.

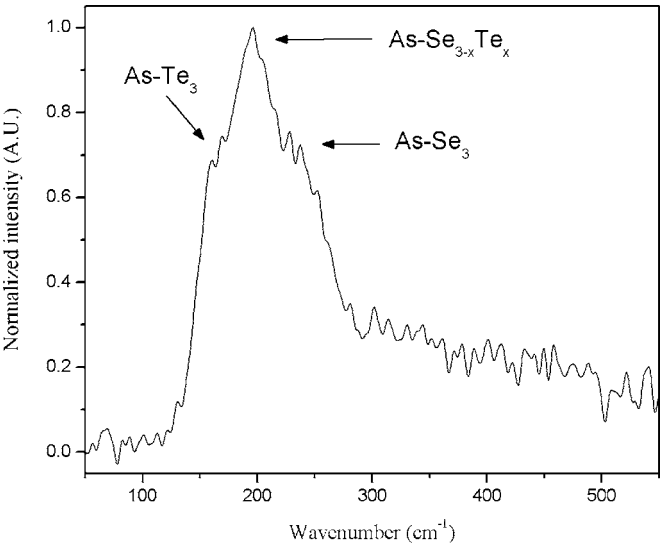

FIG. 2. Micro-Raman spectra of bulk sample with $x=0.15$ in $(1-x)$ $As_{0.40}Se_{0.35}Te_{0.25}+x$ Cu. The spectra exhibit a broad band from 100 to 300 cm^{-1}. This band may be attributed to modified structural units which are represented by $AsSe_{(3-x)}Te_x$ structural units. The shoulders at smaller wave number may be attributed to Te concentrated $AsSe_{(3-x)}Te_x$ units, as Te is heavier than Se. Two shoulders are visible, one at 170 cm^{-1}, which is consistent with the features that appear in pure As_2Te_3 glasses and is probably due to $AsTe_3$ units existing in the glasses, and another at ~240cm^{-1}, which may be related to $AsSe_3$ pyramidal units. No variation of the Raman signal was observed when the Cu content increases. This may suggest that Cu is introduced into the glass without disrupting the basic network structure.

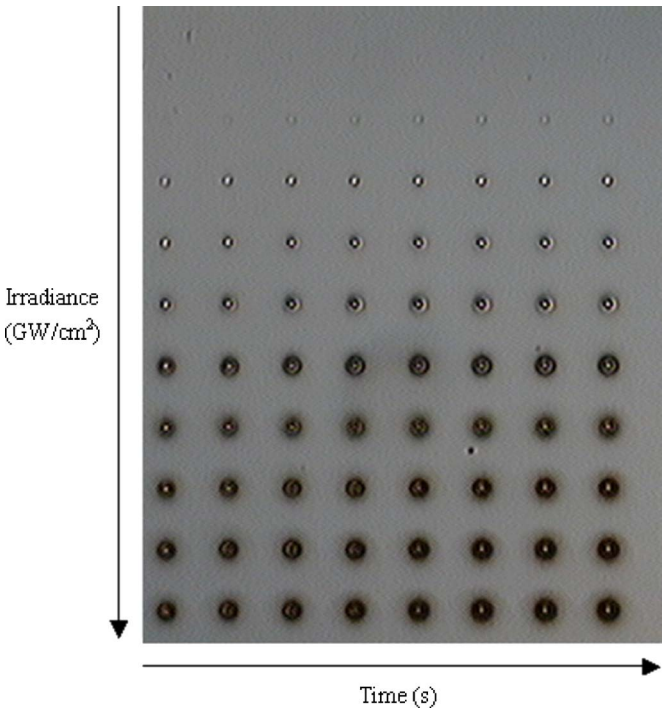

FIG. 3. Microscope image of the glass with $x=0.05$ in $(1-x)$ $As_{0.40}Se_{0.35}Te_{0.25}+x$ Cu, utilizing a 50× microscope objective. Apparent is the systematic variation in material response, as noted by the exposed region's appearance, as a function of irradiance. The ablation threshold appears to be a function of only the laser intensity. No dependence with the irradiance or accumulated number of laser shots for a given exposure time can be observed. The threshold between ablation and photoinduced writing has been estimated for the glass with $x=0.05$ to be ~3 GW/cm^2.

The response of the investigated bulk samples under IR laser irradiation has been tested using IR femtosecond laser exposure in order to determine the maximum transmittable laser power before the degradation of the bulk sample. The threshold for the onset of ablation as compared to nonablative photomodification was determined by irradiating separated spots with a specific number of pulses, followed by incrementally increasing the laser intensity resulting in a two-dimensional map. Figure 3 shows a photomicrograph map of these spots for the glass with $x=0.05$, utilizing a 50 × microscope objective. Apparent is the systematic variation in material response, as noted by the exposed region's appearance, as a function of irradiance. The ablation threshold appears to be a function of the laser intensity. No dependence with the irradiance or accumulated number of laser shots for a given exposure time can be observed. The threshold between ablation and photoinduced writing has been estimated for the glass with $x=0.05$ to be ~3 GW/cm^2. Similar determination of the ablation thresholds for the other glasses investigated is shown in Fig. 4 as a function of the Cu content and clearly demonstrates that the ablation threshold de-

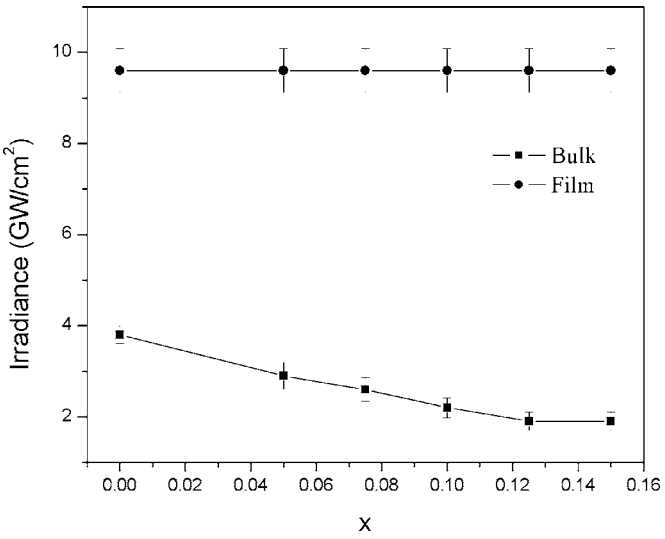

FIG. 4. Ablation threshold as a function of the Cu content in $(1-x)$ $As_{0.40}Se_{0.35}Te_{0.25}+x$ Cu glasses. The ablation threshold decreases dramatically with the progressive incorporation of Cu in the glass network. This is attributed to the redshift of the absorption band gap with an increase of x, as presented in Fig. 1.

creases dramatically with the progressive incorporation of Cu in the glass network. This can be attributed to the redshift of the absorption band gap with an increase of x, as presented in Fig. 1.

The conductance of the investigated glasses has been measured at temperatures ranging from room temperature down to 70 K. Table I lists the conductivity of the glasses (measured at 298 K) and clearly shows that the conductivity increases by a factor of 35 when the content of Cu increases from $x=0.075$ to $x=0.15$. This is in agreement with previous work on the measurement of conductivity of Cu doped As_2Se_3.[19] Kolomiets *et al.* show that the addition of up to 0.2 at. % decreases the conductivity with an increase of activation energy due to an increase in carrier scattering by lattice imperfections caused by the impurity.[20] A further increase in Cu content up to 2.4 at. % results in a decrease in activation energy and an increase in conductivity. Fraser and Owen have demonstrated that this trend continues for alloys with up to 27 at. %.[21] The logarithms of the conductivity data are plotted against both $1/T$ and $T^{-1/4}$ and are presented, respectively, in Figs. 5(a) and 5(b). These results have been fitted considering two conduction mechanisms: extended state conduction which is equivalent to thermal excitation of localized carriers into the bands and variable range hopping near the Fermi level. The fits are also shown in Figs. 5(a) and 5(b). As one can see, below 200 K, the conductance of all the samples can be very well fitted to the $T^{-1/4}$ law. This excellent fit indicates that carrier hopping near Fermi level is most probably the dominant charge transport mechanism at low temperature, which is consistent with the general trend that the $T^{-1/4}$ law is obeyed at lower temperature.[15]

According to the discussions by Ambegaokar *et al.*[22] and Paul and Mitra,[23] electron localization parameter α and density of states near Fermi energy $N(E_F)$ can be calculated using

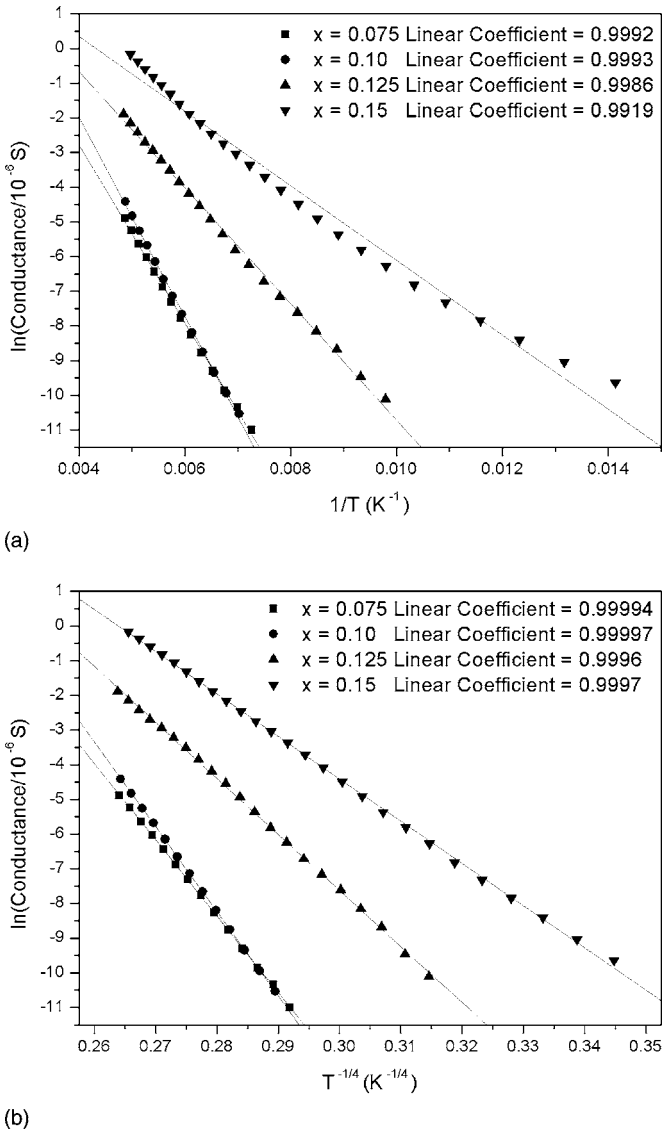

FIG. 5. Conductance of the bulk $(1-x)$ $As_{0.40}Se_{0.35}Te_{0.25}+x$% Cu glasses at temperatures ranging from 200 to 70 K fitted to two different conduction models: (a) ln(conductance)-$1/T$, extended state conduction or thermal excitation of localized states; (b) ln(conductance)-$T^{1/4}$, variable range hopping according to the Mott-Davis model. The error of the measurement is estimated to be smaller than 1 pS.

$$\alpha(\mathrm{cm}^{-1}) = \left(\frac{21.22\times 10^{13}}{\nu_{ph}^3}\right)\sigma_0 T^{1/2} T_0^{1/2}, \tag{2}$$

$$N(E_F)(\mathrm{cm}^{-3}\,\mathrm{eV}^{-1}) = \frac{1.996\times 10^{48}}{\nu_{\mathrm{ph}}}(\sigma_0 T^{1/2})^3 T_0^{1/2}, \tag{3}$$

where $\sigma_0 T^{1/2}$ is the intercept of $\ln(\sigma T^{1/2})-T^{-1/4}$ curve, T_0 is the proportionality defined in Eq. (1), and ν_{ph} is the characteristic phonon frequency taken as 10^{12} Hz, a typical value in amorphous materials.[24]

The calculation results are tabulated in Table II. If we use the preexponential factor $\sigma_0 T^{1/2}$ fitted from the $\ln(\sigma T^{1/2})-T^{-1/4}$ curve, the calculation gives an unphysically high value of $N(E_F)$ compared to Mott *et al.*[19] who found $10^{17}-10^{19}$ cm^{-3} defect centers in chalcogenide glasses. This phenomenon was attributed to the oversimplified assumptions [e.g., constant density of states (DOS) near Fermi en-

TABLE II. Mott's parameters α and $N(E_F)$ calculated for bulk $(1-x)$ $As_{0.40}Se_{0.35}Te_{0.25}+x$ Cu glasses using a typical phonon frequency of 10^{12} Hz. $^*N(E_F)$ were density of states near Fermi energy calculated by assuming $\alpha=(10\ \text{Å})^{-1}$.

x	$\sigma_0 T^{1/2}$ $(\Omega^{-1}\ \text{cm}^{-1}\ \text{K}^{1/2})$	T_0 (K)	α (cm^{-1})	$N(E_F)$ $(\text{cm}^{-3}\ \text{eV}^{-1})$	$^*N(E_F)$ $(\text{cm}^{-3}\ \text{eV}^{-1})$
0.075 $As_{0.37}Se_{0.33}Te_{0.23}Cu_{0.075}$	9.95×10^{19}	2.63×10^{9}	1.08×10^{27}	1.01×10^{77}	7.04×10^{16}
0.1 $As_{0.36}Se_{0.32}Te_{0.23}Cu_{0.10}$	8.14×10^{22}	3.91×10^{9}	$1.079\,18\times10^{30}$	6.72×10^{85}	4.75×10^{16}
0.125 $As_{0.35}Se_{0.31}Te_{0.21}Cu_{0.125}$	4.00×10^{14}	7.97×10^{8}	2.40×10^{21}	3.60×10^{60}	2.33×10^{17}
0.15 $As_{0.34}Se_{0.30}Te_{0.21}Cu_{0.15}$	7.63×10^{10}	2.74×10^{8}	2.68×10^{17}	1.47×10^{49}	6.76×10^{17}

ergy, omission of multiphonon process, etc.] which Mott used in deriving his variable range hopping theory.[15,25] A more reasonable estimation of $N(E_F)$ can be given by assuming $\alpha\sim(10\ \text{Å})^{-1}$ (a value comparable to a few atomic spacings in glasses[19]) in the equation

$$N(E_F)=\frac{16\alpha^3}{kT_0}. \tag{4}$$

This assumption leads to a defect density of the order of $10^{16}-10^{17}\ \text{cm}^{-3}\ \text{eV}^{-1}$. The conductance of $x=0.075$ and $x=0.10$ samples can also be reasonably fitted to an Arrhenius-type temperature dependence, which suggests a mixture of hopping and band conduction in the temperature range of the measurement. The Arrhenius temperature dependence may be attributed to a larger defect density of states near the Fermi level in the two Cu-rich samples, increasing the likelihood of variable range hopping.

2. Single-source film deposition

The films were obtained by single-source thermal deposition technique using the investigated bulk glasses as an evaporation source. Current and power were monitored as a function of boat material, boat size, and amount of glass inside the boat, to maintain a constant evaporation rate of 15 Å/s. Table III summarizes the film thickness measured using a P10 Tencor surface profiler, and film composition was measured using WDS elemental analysis.

X-ray diffraction results (not shown here) confirm the amorphous nature of the films. The compositional analysis of the single-source evaporated films from the different bulk samples indicates that no Cu has been incorporated into the films, leading to the conclusion that Cu did not evaporate congruently with other low-melting point elements during the single-source evaporation. This phenomenon may be explained by the comparatively low vapor pressure of Cu (compared to volatile As and chalcogens), at the evaporation temperature. Due to the absence of Cu, the films do not maintain the compositional stoichiometry of the bulk source. A significant content of Te has been measured in all the films. Cross-sectional WDS elemental analysis reveals an elemental concentration gradient across a 16.5 μm thick film (Fig. 6). The film was striated into three or more layers, starting from an As-rich layer near the substrate and gradually turned to a Te-rich surface layer. Similar trends have

TABLE III. Composition analysis and thickness of the Cu doped films obtained by the single-source evaporation of the Cu doped bulk. The thicknesses of the films were measured using a P10 Tencor surface profiler.

x	Thickness (μm) ±0.1 μm	At. % of actual film composition ±1%		
		As (%)	Se (%)	Te (%)
0.05 $As_{0.38}Se_{0.33}Te_{0.24}Cu_{0.05}$		17	31	52
0.075 $As_{0.37}Se_{0.33}Te_{0.23}Cu_{0.075}$	9.2	18	30	52
0.1 $As_{0.36}Se_{0.32}Te_{0.23}Cu_{0.10}$	16.5	13	29	59
0.125 $As_{0.35}Se_{0.31}Te_{0.21}Cu_{0.125}$	12.2	16	31	53
0.15 $As_{0.34}Se_{0.30}Te_{0.21}Cu_{0.15}$	26.9	25	32	43

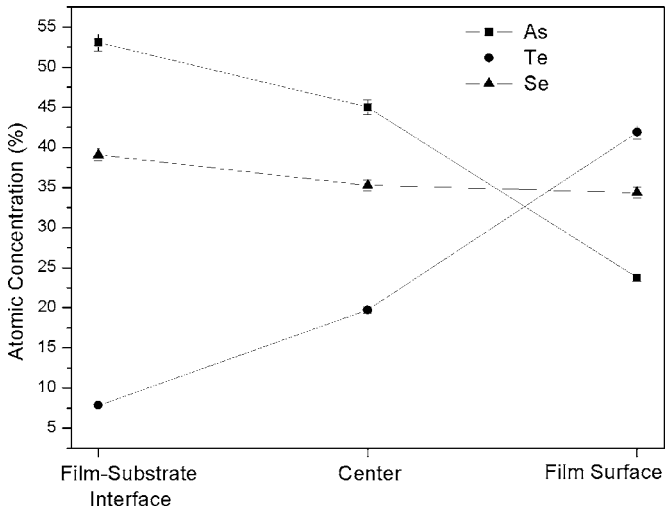

FIG. 6. WDS elemental analysis results confirming the As-rich bottom layer which gradually turned into a Te-rich surface layer.

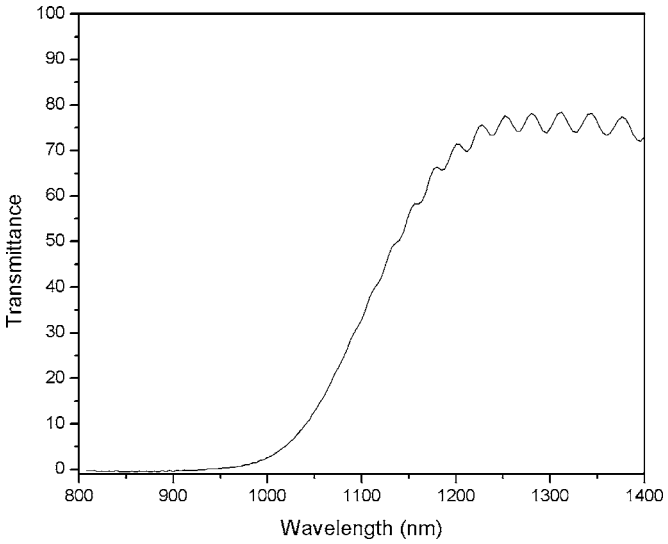

FIG. 7. Transmission spectra of the film with $x=0.10$ obtained using the thermal deposition process taken as an example as the transmission spectra for all the films are similar owing to their comparable compositions.

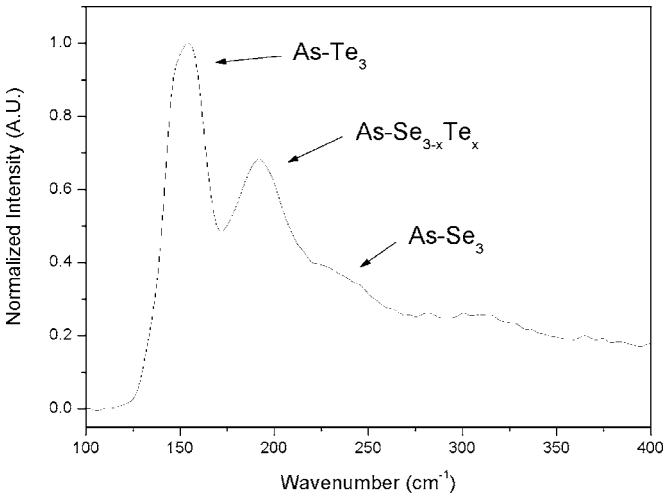

FIG. 8. Micro-Raman spectra of the film with $x=0.10$, taken as an example, obtained using thermal deposition process. The Raman spectrum is dominated by the band at 170 cm^{-1}, which confirms the presence of excess Te units at the surface of the films in accordance with the WDS data in Fig. 6. A similar micro-Raman spectrum, which differs from the ones of the corresponding bulk samples (Fig. 2), has been measured for all the single-source evaporated films.

been observed in the other $(1-x)$ $As_{0.40}Se_{0.35}Te_{0.25}+x$ Cu films when evaporated from bulk glass sample using the single-source evaporation technique. This can be attributed to volatile As being preferentially evaporated from the melt, forming the As-rich bottom layer resulting in the depletion of As in the source, and hence the decreased As content in the films, thereafter during the course of the evaporation.

The optical transmission spectrum of the film with $x=0.10$ is displayed in Fig. 7 along with their upper and lower envelopes. The transmission spectra for all the films are similar owing to their comparable compositions. However, we have observed that the distance between the fringes is not the same. This has to be related to the thickness of the films. Indeed, it is very well known that (i) the upper and lower interference envelopes are dependent on the refractive index and (ii) the distance between the fringes is dependent on both the refractive index and the thickness of the films.[26]

The micro-Raman spectrum of the film with $x=0.10$ is exhibited in Fig. 8. The spectrum exhibits two broad bands centered at 160 and 195 cm^{-1}. As explained previously, the presence of the band at 170 cm^{-1} indicates the presence of $AsTe_3$ units and the band at 195 cm^{-1} indicates the presence of $AsSe_{(3-x)}Te_x$ structural units. The shoulder at ~240 cm^{-1} shows the existence of some $AsSe_3$ pyramidal units in the glass network. As the Raman spectra are dominated by the band at 170 cm^{-1}, this confirms the presence in excess of Te units at the surface of the films in accordance with the WDS analysis when measured at the surface of the film. A similar micro-Raman spectrum has been measured for the single-source evaporated films. However, this spectrum differs from the ones of the corresponding bulk samples (Fig. 2).

The irradiation test at 800 nm using an IR laser source has been performed on the films. The ablation threshold for all the films occurs at around 9.6 GW/cm^2 and is higher than that of the corresponding bulk, which can be attributed to a redshift of the absorption edge of the films compared to the bulk. Furthermore, the similarity in ablation threshold between all films implies that the films have similar compositions.

B. Dual-source coevaporation for obtaining As–Se–(Te)–Cu films

To deposit films with high Cu concentrations, we have investigated a dual-source coevaporation technique for film deposition. The composition nonuniformity due to noncongruent evaporation has been minimized by equilibrating the evaporation source prior to deposition. Instead of exhausting all the bulk materials loaded into the boats which leads to compositionally striated films, we carried out the deposition only when the evaporation reached a steady state, namely, a constant deposition rate is maintained at a fixed current value. Table IV lists the compositional analysis of the dual-source coevaporated films. $(As_2Se_3)_{100-x}(CuSe)_x$ $(x=8,30)$ films were codeposited simultaneously from As_2Se_3 and CuSe sources, while $(As_2Se_3)_{100-x}(CuSe)_x$ $(x=40,60)$ films were obtained by coevaporating from As_2Te_3 and CuSe sources. The nominal compositions of the films were estimated from the individual deposition rates of As-ChG and Cu-ChG sources. From Table IV, one can notice that the films $(As_2Se_3)_{92}(CuSe)_8$ and $(As_2Se_3)_{70}(CuSe)_{30}$ films have a similar composition within the accuracy of the WDS measurement (±1 at. %), whereas the seleno-tellurite films have the expected composition.

Figure 9 shows the transmission spectra of the coevaporated films. An increase of Cu content in the $(As_2Se_3)_{92}(CuSe)_8$ and $(As_2Se_3)_{70}(CuSe)_{30}$ films shifts the position of the band gap to higher wavelength. This is in good agreement with the redshift of the absorption band gap observed in bulk glasses in the As–Se–Te–Cu system (Fig. 1). The absorption edge of $(As_2Te_3)_{40}(CuSe)_{60}$ is situated at shorter wavelength compared to the one of the

TABLE IV. Composition analysis and thickness of the Cu doped films obtained by coevaporation technique.

Nominal film composition	Conductivity [1/(Ω m)] at 293 K	Thickness (μm) ±0.1 μm	At. % of actual film composition ±1%			
			As (%)	Se (%)	Te (%)	Cu (%)
$(As_2Se_3)_{92}(CuSe)_8$ $As_{0.387}Se_{0.597}Cu_{0.016}$	0.000 15	4.5	33	57		10
$(As_2Se_3)_{70}(CuSe)_{30}$ $As_{0.342}Se_{0.585}Cu_{0.073}$	0.006 93	5.6	30	53		17
$(As_2Te_3)_{60}(CuSe)_{40}$ $As_{0.316}Se_{0.105}Cu_{0.105}Te_{0.474}$	0.021 28	0.2	26	18	50	6
$(As_2Te_3)_{40}(CuSe)_{60}$ $As_{0.25}Se_{0.188}Cu_{0.188}Te_{0.375}$	0.203 64	0.7	18	42	24	16

$(As_2Te_3)_{60}(CuSe)_{40}$ film. This is attributed to the lower Te content which blueshifts the band gap counteracting the Cu doping effect.

The micro-Raman spectra of the coevaporated films are shown in Fig. 10. The spectra exhibit bands, the intensity of which depends on the composition of the film, located at 150, 195, and 230 cm^{-1}. As seen in the Raman spectra of the Cu doped bulk glasses in the As–Se–Te system, the band at 150 cm^{-1} has been related to $AsTe_3$ units, the one at 195 cm^{-1} to mixed units $AsSe_{(3-x)}Te_x$, and the one at 230 cm^{-1} to $AsSe_3$ pyramidal units. The following observations are made.

(i) The $(As_2Se_3)_{92}(CuSe)_8$ and $(As_2Se_3)_{70}(CuSe)_{30}$ films exhibit a similar Raman signal. This is attributed to the similarity in their composition.

(ii) The films with compositions of $(As_2Te_3)_{60}(CuSe)_{40}$ and $(As_2Te_3)_{40}(CuSe)_{60}$ present different Raman signals. The spectrum of the $(As_2Te_3)_{60}(CuSe)_{40}$ film exhibits a Raman spectrum dominated by the band at 150 cm^{-1} which is consistent with the highest Te content. The spectrum of the Se-rich $(As_2Te_3)_{40}(CuSe)_{60}$ film is dominated by the band at 195 cm^{-1}. Due to its higher Se content, the band at 230 cm^{-1}, which is related to the vibration of Se based units, is more pronounced compared to the one measured in the $(As_2Te_3)_{60}(CuSe)_{40}$ film.

The electrical properties of the $(As_2Te_3)_{60}(CuSe)_{40}$ and $(As_2Te_3)_{40}(CuSe)_{60}$ films have been measured. As seen for the Cu doped glasses and as shown in Table IV, the conductivity of the films measured at 293 K increases with an increase of Cu content. Figures 11(a) and 11(b) show plots of the logarithm of the conductance data versus $-1/T$ and $T^{1/4}$, respectively. As seen in Fig. 11(b), the logarithm of the conductance of the $(As_2Te_3)_{40}(CuSe)_{60}$ films can be very well fitted to the $T^{-1/4}$ law with a linear coefficient as high as 0.9997. As explained previously, this indicates that carrier hopping near the Fermi level dominates the charge transport mechanism at low temperature. Assuming that a localization parameter $\alpha=(10\ Å)^{-1}$ yields the DOS near E_F of 1.00

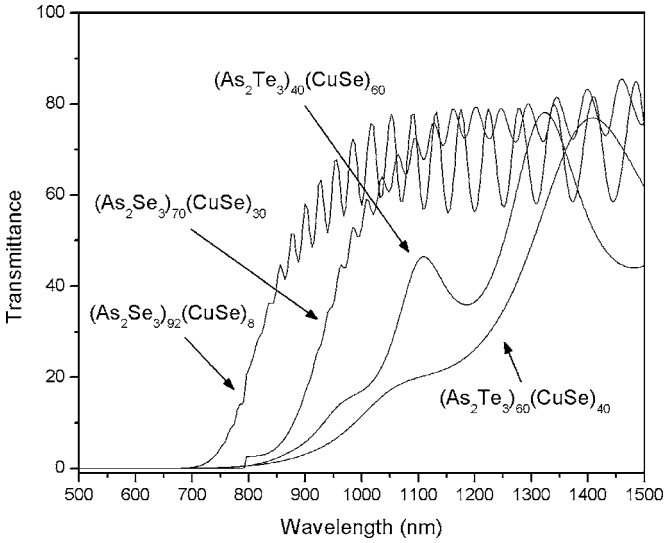

FIG. 9. Transmission spectra of the Cu doped coevaporated films. An increase of Cu content in the $(As_2Se_3)_{92}(CuSe)_8$ and $(As_2Se_3)_{70}(CuSe)_{30}$ films shifts the position of the band gap to longer wavelength. The absorption edge of $(As_2Te_3)_{40}(CuSe)_{60}$ is situated at shorter wavelength compared to the one of the $(As_2Te_3)_{60}(CuSe)_{40}$ film. This is attributed to the lower Te content which blueshifts the band gap counteracting the Cu doping effect.

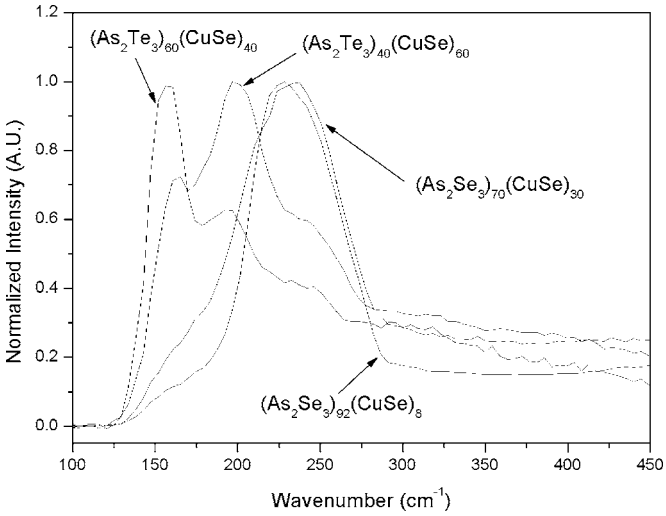

FIG. 10. Micro-Raman spectra of the Cu doped coevaporated films. The spectra exhibit different bands, the intensity of which depends on the composition of the film.

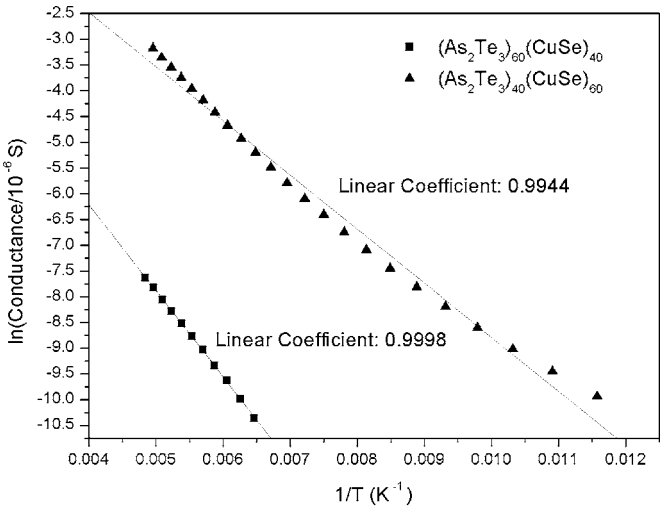

(a)

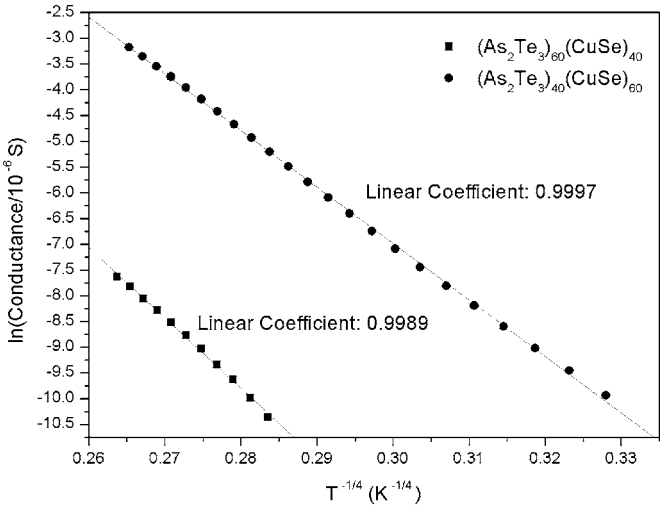

(b)

FIG. 11. Conductance of $(As_2Te_3)_{40}(CuSe)_{60}$ and $(As_2Te_3)_{60}(CuSe)_{40}$ films at low temperature fitted to different conduction models: (a) ln(conductance)-$-1/T$, extended state conduction or thermal excitation of localized states; (b) ln(conductance)-$T^{1/4}$, variable range hopping according to the Mott-Davis model. The error of the measurement is estimated to be smaller than 1 pS.

$\times 10^{19}$ cm^{-3} eV^{-1} for $(As_2Se_3)_{40}(CuTe)_{60}$. However, the logarithm of the conductance of the $(As_2Te_3)_{60}(CuSe)_{40}$ film can be reasonably fitted with both models, suggesting a mixture of the two conduction mechanisms, which again can be attributed to the lower defect density in this glass film.

IV. CONCLUSION

In this paper, we systematically studied the chemical modification of As–Se–Te glass systems incorporated with Cu. It was found that incorporation of Cu into the glass network increases T_g, the density, and the electrical conductivity at low temperature and, also, shifts the absorption band gap to longer wavelength.

We have shown that it is not possible to deposit Cu doped films with high Cu concentrations from bulk samples when this material is used as the single source in a thermal evaporator. The films were found to have a laminated compositionally nonuniform structure in thick films. We have demonstrated that significant Cu content can be incorporated into selenide or seleno-telluride glass network by coevaporating As–Se–Te and Cu-ChG systems.

The electrical conductivity properties have been measured in Cu doped bulks and films and we have observed an increase in the electrical conductivity at low temperature with an increase of Cu content. We have found that the charge transport mechanism at low temperature is dominated by carrier hopping near Fermi level. Such electrical properties will allow further evaluation of these Cu doped ChGs as candidates for low-cost mid-IR detection materials.

[1] Y. Vlasov, Y. Ermolenko, A. Legin, and Y. Murzina, J. Anal. Chem. USSR **54**, 476 (1999).
[2] A. Zakery and S. Elliott, J. Non-Cryst. Solids **330**, 1 (2003).
[3] J. Sanghera and I. Aggarwal, J. Non-Cryst. Solids **256–257**, 6 (1999).
[4] I. Aggarwal and J. Sanghera, J. Optoelectron. Adv. Mater. **4**, 665 (2002).
[5] J. Viens, C. Meneghini, A. Villeneuve, T. Galstian, E. Knystautas, M. Duguay, K. Richardson, and T. Cardinal, J. Lightwave Technol. **17**, 1184 (1999).
[6] Y. Ruan, W. Li, R. Jarvis, N. Madsen, A. Rode, and B. Luther-Davies, Opt. Express **12**, 5140 (2004).
[7] T. Galstyan, J. Viens, A. Villeneuve, K. Richardson, and M. Duguay, J. Lightwave Technol. **15**, 1343 (1997).
[8] H. Y. Hwang, G. Lenz, M. E. Lines, and R. E. Slusher, U.S. Patent No. 6,208,792 (27 March 2001).
[9] D. Hewak, *Progress Towards A* 1300 nm *Fiber Amplifier* (The Institution of Electrical Engineers, Savoy Place, London WCPR OBL, UK, 1998).
[10] A. K. Campbell, U.S. Patent No. 20030047765 (pending).
[11] T. Carrig, J. Electron. Mater. **31**, 759 (2002).
[12] S. Lukic, D. Petrovic, I. Turyanitsa, and O. Khiminets, J. Mater. Sci. **26**, 5517 (1991).
[13] E. Mytilineou, J. Optoelectron. Adv. Mater. **4**, 705 (2002).
[14] V. Lyubin, M. Klebanov, M. Mitkova, and T. Petkova, Appl. Phys. Lett. **71**, 2118 (1997).
[15] *Amorphous Semiconductors*, Topics in Applied Physics Vol. 36, edited by M. Brodsky (Springer-Verlag, New York 1979).
[16] W. Li *et al.*, J. Appl. Phys. **98**, 053503 (2005).
[17] T. Usuki, K. Saitoh, M. Endo, and O. Uemura, J. Non-Cryst. Solids **205–207**, 184 (1996).
[18] V. Nguyen, J. Sanghera, J. Freitas, I. Aggarwal, and I. Lloyd, J. Non-Cryst. Solids **248**, 103 (1999).
[19] N. Mott and E. Davis, *Electronic Processes in Non-Crystalline Materials* (Clarendon Press, New York Oxford University Press, 1979).
[20] B. Kolomiets, Y. Rukhyladev, and V. Shilo, J. Non-Cryst. Solids **5**, 402 (1971).
[21] M. Fraser and A. Owen, J. Non-Cryst. Solids **59–60**, 1031 (1983).
[22] V. Ambegaokar, B. Halperin, and J. Langer, Phys. Rev. B **4**, 2612 (1971).
[23] D. Paul and S. Mitra, Phys. Rev. Lett. **31**, 1000 (1973).
[24] M. Dongol, M. Zied, G. Gamal, and A. El-Denglawey, Appl. Surf. Sci. **161**, 365 (2000).
[25] H. Overhof, in *Festkorperprobleme XVI*, edited by J. Treusch (Vieweg & Sohn, Braunschweig, Germany, 1976), p. 239.
[26] R. Swanepoel, J. Phys. E **16**, 1214 (1983).